ARTICLES

High Resolution Photofragment Translational Spectroscopy Studies of the Ultraviolet Photolysis of Phenol-d_5

Graeme A. King, Thomas A. A. Oliver, Michael G. D. Nix, and Michael N. R. Ashfold*

School of Chemistry, University of Bristol, Bristol BS8 1TS, U.K.

Received: April 6, 2009; Revised Manuscript Received: May 18, 2009

The dissociation dynamics of gas phase phenol-d_5 molecules (C_6D_5OH) following excitation at numerous wavelengths in the range $275 \geq \lambda_{phot} \geq 193.3$ nm have been investigated using the techniques of H (Rydberg) atom photofragment translational spectroscopy and resonance enhanced multiphoton ionization spectroscopy. The results are compared with those from recent studies of the fully hydrogenated and fully deuterated isotopologues (C_6H_5OH and C_6D_5OD), and various halo- and methyl-substituted phenols. Analysis of the vibrational energy disposal within the phenoxyl-d_5 dissociation products identifies three distinct O−H bond fission pathways, involving nonadiabatic coupling to dissociative states of $^1\pi\sigma^*$ character, following initial $\pi^* \leftarrow \pi$ excitation. Dissociation at $\lambda_{phot} > 248$ nm involves internal conversion (IC) to high vibrational levels of the electronic ground ($^1\pi\pi$) state and subsequent coupling to the lowest $^1\pi\sigma^*$ potential energy surface (PES) via a conical intersection (CI) between the $^1\pi\pi/^1\pi\sigma^*$ PESs at extended O−H bond lengths (R_{O-H}). Once $\lambda_{phot} \leq 248$ nm, dissociation proceeds directly, via a $^1\pi\pi^*/^1\pi\sigma^*$ CI. Both pathways yield phenoxyl-d_5 products in selected vibrational levels of the ground ($\tilde{X}^2B_1$) electronic state. The detailed energy disposal within the phenoxyl-$d_5(\tilde{X})$ products shows many parallels with that deduced from companion studies of other phenol isotopologues and various substituted phenols, but a notable isotope effect is identified, thus providing yet greater insights into the factors controlling the vibrational energy disposal in the phenoxyl products. A hitherto unobserved O−H bond fission channel yielding phenoxyl-d_5 fragments in the electronically excited $\tilde{B}^2A_2$ state is identified at the shortest excitation wavelength ($\lambda_{phot} = 193.3$ nm) and rationalized in terms of nonadiabatic coupling to, and subsequent dissociation on, the second excited $^1\pi\sigma^*$ PES. Selective deuteration as in phenol-d_5 causes little reduction in the intensity of the "slower" H atom products that are observed from all phenol systems, suggesting that C−H/D bond fission makes at most a minor contribution to this feature.

1. Introduction

Phenol is the chromophore of the amino acid tyrosine and its photochemistry has thus been the subject of extensive experimental[1−6] and theoretical studies.[7−10] Phenol exhibits strong ultraviolet (UV) absorption associated with $\pi^* \leftarrow \pi$ excitations, but low fluorescence quantum yields,[11] indicating the operation of one or more nonradiative decay mechanisms from the photoexcited state(s). One such mechanism involves deactivation via a $^1\pi\sigma^*$ potential energy surface (PES), which is dissociative along the O−H stretch coordinate, R_{O-H}.[9] This state arises from a 3s $\leftarrow \pi$ excitation in the vertical Franck−Condon (vFC) region, but the 3s (Rydberg) electron density evolves into an antibonding σ^* orbital upon extending R_{O-H}. In what follows, descriptors like $^1\pi\pi$, $^1\pi\pi^*$, $^1\pi\sigma^*$, etc. are used to represent diabatic states, while the adiabatic PESs are denoted by S_0, S_1, S_2, etc. As Figure 1 illustrates, the first $^1\pi\sigma^*$ state in phenol is the second excited singlet state in the vFC region and exhibits conical intersections (CIs) with both the $^1\pi\pi^*$ and $^1\pi\pi$ PESs.

O−H bond fission in phenol-h_6 has been investigated following excitation at many wavelengths in the range $206 \leq \lambda_{phot} \leq 280$ nm using the H (Rydberg) atom photofragment translational spectroscopy (PTS) technique.[2] The resulting total kinetic energy release (TKER) spectra all show a fast, structured component, attributable to H atom loss by dissociation on the first $^1\pi\sigma^*$ PES, analysis of which reveals that the phenoxyl products are formed with very specific vibrational excitation. Two O−H bond fission mechanisms were identified that yield fast H atom products,[2] both of which are illustrated in Figure 1. Excitation at long wavelengths ($\lambda_{phot} > 248$ nm) populates $^1\pi\pi^*$ levels at energies below the first $^1\pi\pi^*/^1\pi\sigma^*$ CI. Dissociation in this case is deduced to proceed via internal conversion (IC) to high vibrational levels of the ground state, and subsequent coupling via the $^1\pi\pi/^1\pi\sigma^*$ CI at extended R_{O-H}. The H + C_6H_5O products display an isotropic recoil velocity distribution, with a mean total kinetic energy release (TKER) ~6000 cm^{-1}. When excitation is at shorter wavelengths ($\lambda_{phot} \leq 248$ nm), O−H bond fission proceeds on a much faster time scale, by direct coupling at the first $^1\pi\pi^*/^1\pi\sigma^*$ CI. The fast H + C_6H_5O products that result are characterized by a mean TKER ~11 500 cm^{-1} and an anisotropic recoil velocity distribution.

TKER spectral analysis shows that the phenoxyl products formed following O−H bond fission in the long wavelength regime often populate short, odd-quanta only, progressions of levels involving the out-of-plane ring puckering mode $\nu_{16a}(a'')$.[2]

* Author for correspondence. Tel: (117)-9288312/3. Fax: (117)-9250612. E-mail: mike.ashfold@bris.ac.uk.

10.1021/jp9031404 CCC: $40.75
Published on Web 06/18/2009

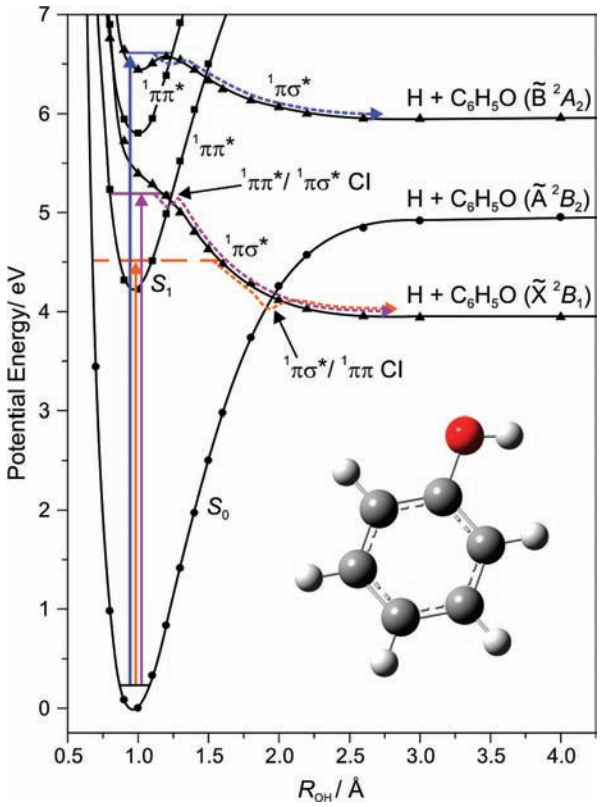

Figure 1. Calculated CASPT2 potential energy cuts through the O−H stretch coordinate (R_{O-H}) for the ground ($^1\pi\pi$) and first two excited $^1\pi\pi^*$ and $^1\pi\sigma^*$ states of phenol, illustrating the first three dissociation limits for H + C_6H_5O. Three possible mechanisms of direct O−H bond fission are highlighted. Two pathways result in the formation of phenoxyl radicals in the ground ($\tilde{X}^2B_1$) state and differ depending upon whether excitation is to energies above (purple dashed line) or below (orange dashed line) the first $^1\pi\pi^*/^1\pi\sigma^*$ CI. A third, hitherto unobserved, pathway is also proposed, characterized by coupling at a higher $^1\pi\pi^*/^1\pi\sigma^*$ CI (blue dashed line) and formation of excited ($\tilde{B}^2A_2$) state phenoxyl products.

[Here, and throughout this Article, we adopt Wilson's labeling scheme[12] for the normal modes of phenol and the phenoxyl radical.] Such specific energy disposal has been rationalized by symmetry arguments. The ground and $^1\pi\pi^*$ states of phenol both have A′ electronic symmetry. Evolution onto the $^1\pi\sigma^*$ PES, of A″ symmetry, at the $^1\pi\pi/^1\pi\sigma^*$ CI thus requires distortion of the nuclear geometry along one or more coupling coordinates of appropriate (a″) symmetry. Theory[9,10] suggests that OH torsion is particularly efficient at promoting such coupling, but the observed population in product mode ν_{16a}, which involves very similar nuclear motion in the parent molecule, has encouraged suggestions[2] that this motion contributes to coupling at the $^1\pi\pi/^1\pi\sigma^*$ CI. Population of mode ν_{18b} (the C−O in-plane wag, of a′ vibrational symmetry) is observed also, in combination with ν_{16a}. This has been attributed to a small change in C−C−O bond angle, possibly amplified by the impulse of the departing H atom.[2] Photoexcitation at energies above the S_1-S_0 origin can access a range of parent skeletal vibrations. In many cases these are seen to map through into the phenoxyl products, essentially acting as "spectator" modes during bond fission. However, phenoxyl radicals formed with excitation at $\lambda_{phot} \leq$ 248 nm, i.e., at energies above the first $^1\pi\pi^*/^1\pi\sigma^*$ CI, are found to exhibit a progression in ν_{18b}, in combination with one quantum of another out-of-plane ring puckering vibration, ν_{16b}. By analogy with behavior seen at longer wavelengths, activity in product mode ν_{16b} was assumed to indicate that this mode assists coupling at the first $^1\pi\pi^*/^1\pi\sigma^*$ CI.

In all TKER spectra, the above fast, structured features rest on a broad underlying component, which maximizes at low TKER (~2000 cm^{-1}). The current consensus identifies two contributors to this background signal. One involves IC from the photoexcited $^1\pi\pi^*$ state and subsequent unimolecular decay on the S_0 PES, yielding slow H atoms and internally excited partner fragments. The other involves unintended multiphoton processes (e.g., multiphoton excitation, resonance enhanced by the $^1\pi\pi^*$ state, to dissociative superexcited states.[13])

Broadly similar dissociation dynamics have been observed for a number of substituted phenols, e.g., 4-fluorophenol[14] and 4-methylphenol,[15] in which the substituent is at the para-position. However, two subtle dynamical differences were identified. First, the para-substituted phenoxyl radicals formed with excitation at long wavelengths are found to populate modes ν_{18b} and ν_{9b}, in combination with (odd-quanta of) mode ν_{16a}. The additional presence of ν_{9b} reflects the fact that the CO moiety can "wag" in-phase (ν_{9b}) or out-of-phase (ν_{18b}) with the substituent. The second difference concerns the energy disposal in the substituted phenoxyl products formed with excitation at energies above the first $^1\pi\pi^*/^1\pi\sigma^*$ CI. TKER spectral analysis reveals population of product modes ν_{18b} and ν_{19a} (built on $v_{16b} = 1$). Population of the ring breathe/C−O stretch mode (ν_{19a}) was rationalized on Franck−Condon grounds; with the benefit of hindsight it is likely that both these modes are also populated in the phenoxyl radicals formed in the short wavelength photolysis of bare phenol, but not recognized on account of the near degeneracy between $3\nu_{18b}$ and ν_{19a}.

The photolysis of fully deuterated phenol (phenol-d_6) has also been studied, using D (Rydberg) atom PTS.[2] TKER spectra recorded at photolysis energies above the first $^1\pi\pi^*/^1\pi\sigma^*$ CI were similar to those obtained for phenol-h_6 (albeit less clearly resolved) but, in contrast to the case with phenol-h_6, no fast structured features were observed with excitation at longer wavelengths. O−H bond fission in phenol-h_6 following excitation at long wavelengths proceeds via IC to the ground state, with O−H stretching overtones acting as acceptor modes in the S_0 state,[16] and subsequent coupling at the $^1\pi\pi/^1\pi\sigma^*$ CI. Two factors (at least) reduce the efficacy of this pathway in the case of phenol-d_6. First, the lower frequency of the O−D stretch vibration reduces its efficiency as an acceptor mode facilitating IC to the S_0 state (as signified by the reported order of magnitude increase in the $^1\pi\pi^*_{v=0}$ fluorescence lifetime (as compared with phenol-h_6)).[16] Second, the lower velocity of the departing D atom could be expected to reduce the efficiency of passage around the $^1\pi\pi/^1\pi\sigma^*$ CI. Hence the experimental finding that O−D bond fission in phenol-d_6 via the $^1\pi\sigma^*$ state only proceeds once the excitation wavelength is sufficiently short to access the first $^1\pi\pi^*/^1\pi\sigma^*$ CI.

This contribution explores further the effects of tuning the phenol parent level density by selective deuteration of just the C−H sites. [To avoid any future ambiguity, phenol-h_6, phenol-d_6 and phenol-d_5 are used here to represent, respectively, the phenol molecule when nondeuterated, fully deuterated, and deuterated only at carbon sites. Thus, O−H bond fission in phenol-h_6 generates phenoxyl-h_5 radicals, while H(D) atom loss from the hydroxyl group of phenol-d_5(-d_6) results in phenoxyl-d_5 products.] Several previous photophysical studies of the phenol-d_5 isotopologue have appeared. It has been investigated previously by picosecond time-resolved IR−UV pump−probe spectroscopy,[17,18] as part of a larger study of intramolecular vibrational redistribution

(IVR) following population of OH and CH stretching vibrations of various phenol isotopologues in their respective S_0 states. IVR rates from the OH stretch mode in phenol-h_6 were found to be 5.7× faster than that in phenol-d_5, suggesting a major role for doorway states composed of CH stretching vibrations in the IVR process. The vapor phase UV absorption spectrum of phenol-d_5 has been reported,[19] and the phenoxyl-d_5 radical has been probed by both Raman and FTIR spectroscopy.[20,21] Recent velocity mapped ion imaging studies of phenol-d_5 photolysis at various wavelengths in the range $212.2 \leq \lambda_{phot} \leq 258.6$ nm[22] found that the broad H atom distribution evident at low TKER (~2000 cm^{-1}) in the case of phenol-h_6 is substantially reduced with phenol-d_5, suggesting that a fraction of this feature in the case of phenol-h_6 originates from C−H bond fission. Ultrafast pump−probe imaging studies of phenol-d_5 photolysis at λ_{phot} = 200 nm have been reported also;[23] the fast and slow H atom products observed in that study are both found to be formed on a <150 fs time scale.

Here, we present the results of a comprehensive study of phenol-d_5 photolysis, including the 1 + 1 resonance enhanced multiphoton ionization (REMPI) spectrum near the $S_1 \leftarrow S_0$ origin of phenol-d_5 and the corresponding H atom photofragment excitation (PHOFEX) spectrum, and high resolution TKER spectra of the H + C_6D_5O products formed at many excitation wavelengths both below and above the energy of the first $^1\pi\pi^*/^1\pi\sigma^*$ CI. Many similarities with the findings from previous studies of other phenol isotopologues and substituted phenols are recognizable, but the present studies also reveal clear isotope effects on the vibrational energy disposal in the phenoxyl radicals (which serve to clarify further the various factors that determine this energy disposal) and shed more light on the origins of the broad unstructured distribution of H atom products (peaking at low TKER) that is observed at all excitation wavelengths. An additional O−H bond fission channel is identified when both phenol-d_5 and phenol-h_6 are excited at λ_{phot} = 193.3 nm. This hitherto unobserved fragmentation pathway, which involves nonadiabatic coupling to, and subsequent dissociation on, the second excited $^1\pi\sigma^*$ PES, results in population of specific vibrational levels of the second excited ($\tilde{B}^2A_2$) state of the phenoxyl-d_5 (-h_5) products.

2. Experimental Section

Phenol-d_5 was obtained commercially (Aldrich ≥98% purity), placed in a Swagelok filter housing positioned behind a pulsed valve, and heated gently to ~50 °C to generate sufficient vapor pressure for seeding in the argon backing gas (~700 Torr).

The experimental setup and procedure was identical to that described previously.[24,25] Briefly, the pulsed photolysis laser radiation intercepted the skimmed, pulsed molecular beam of phenol-d_5 in Ar. The composition of the molecular beam was interrogated by inserting a small time-of-flight (TOF) mass spectrometer around the interaction region and monitoring the 1 + 1 REMPI spectrum for phenol-d_5 as a function of photolysis laser wavelength in the range $275 > \lambda_{phot} > 264$ nm. Introducing Lyman-α (121.6 nm/82259 cm^{-1}) radiation (plus the 364.7 nm fundamental radiation from which it is derived, by third harmonic generation in a phase matched Kr/Ar mixture) a short (δt ~10 ns) time after the photolysis laser pulse allowed measurement of the associated H atom PHOFEX spectrum.

H (Rydberg) atom PTS studies required the introduction of an additional laser pulse (with wavelength ~366 nm), synchronous with the Lyman-α radiation. The 121.6 and 366 nm laser pulses induce two photon double resonant excitation of neutral H atom fragments, via the $n = 2$ state, to states with high ($n \sim 80$) principal quantum number, thereby enabling measurement of H (Rydberg) atom TOF spectra. An applied dc field (20 V cm^{-1}) ensured extraction of all prompt H^+ ions (formed by two-color (Lyman-α plus a fundamental photon) absorption) from the interaction region. The D atom TOF spectra were also recorded, by tuning to resonance with the D atom Lyman-α transition (82280 cm^{-1}). The polarization vector (ε_{phot}) of the photolysis radiation could be aligned at any angle (θ) relative to the TOF axis using a polarization rotator. As before,[24] H atom recoil anisotropies were investigated by collecting H atom TOF spectra with ε_{phot} aligned at, respectively, $\theta = 0°$, 54.7° and 90°.

3. Computational Methods

Ab initio potential energy cuts through the O−H stretch coordinate were calculated for the ground state, and the first two $^1\pi\pi^*$ and $^1\pi\sigma^*$ states using complete active space self-consistent field (CASSCF) and complete active space with second-order perturbation theory (CASPT2) methods in MOLPRO Version 2006.1.[26] R_{O-H} was stretched and then fixed while the rest of the geometry was optimized using CASSCF(12/11)/aug-cc-pVTZ[27] for all states shown. CASPT2(12/11)/aug-cc-pVTZ single point energies were then calculated at these optimized geometries (freezing the carbon and oxygen 1s electrons). Intruder state problems were encountered in the CASPT2 calculations, leading to explosions of wave function and no convergence. A small imaginary level shift, as described by Roos et al.[28] was required to remove these and led to normal convergence of excited state wave functions. The active space for both CASSCF and CASPT2 calculations comprised the three benzene π and corresponding π^* orbitals, the π lone pair of the oxygen atom, and two σ orbitals and their corresponding σ^* orbitals. Cuts through the resulting PESs were displayed in Figure 1.

The true energy of the S_1-S_0 origin is underestimated using a 12/11 active space but can be reproduced more accurately using a 10/9 active space. However, only with the larger active space was it possible to capture properly the second $^1\pi\pi^*$ and $^1\pi\sigma^*$ excited states. The present calculations predict the observed O−H bond strength and the threshold energies for the first and second $^1\pi\pi^*/^1\pi\sigma^*$ CIs well. The predicted $T_{00}(\tilde{A}-\tilde{X})$ and $T_{00}(\tilde{B}-\tilde{X})$ separations in the radical are also in good accord with the experimental values.[29]

4. Results

As with phenol-h_6, the REMPI-TOF mass spectrum obtained upon tuning to the wavelength of the S_1-S_0 origin of phenol-d_5 (λ_{phot} = 273.815 nm) is dominated by the parent ion peak (m/z 99), with only small amounts of fragmentation products. A peak at m/z 1 (H^+) is only observed following addition of the 121.6 nm radiation (and the fundamental wavelength from which it derives). As Figure 2 shows, the wavelength resolved 1 + 1 REMPI spectrum of phenol-d_5 in this region, and the corresponding H atom PHOFEX spectrum, are both structured and mirror one another closely. These spectra have been assigned primarily with reference to the vapor phase absorption spectra reported by Bist et al.,[19] assisted by the results from H (Rydberg) atom PTS measurements, as described later. These assignments are summarized in Table 1.

TOF spectra of H-atom fragments resulting from photolysis of phenol-d_5 were recorded at wavelengths corresponding to several of the major resonances identified in Figure 2a. TOF

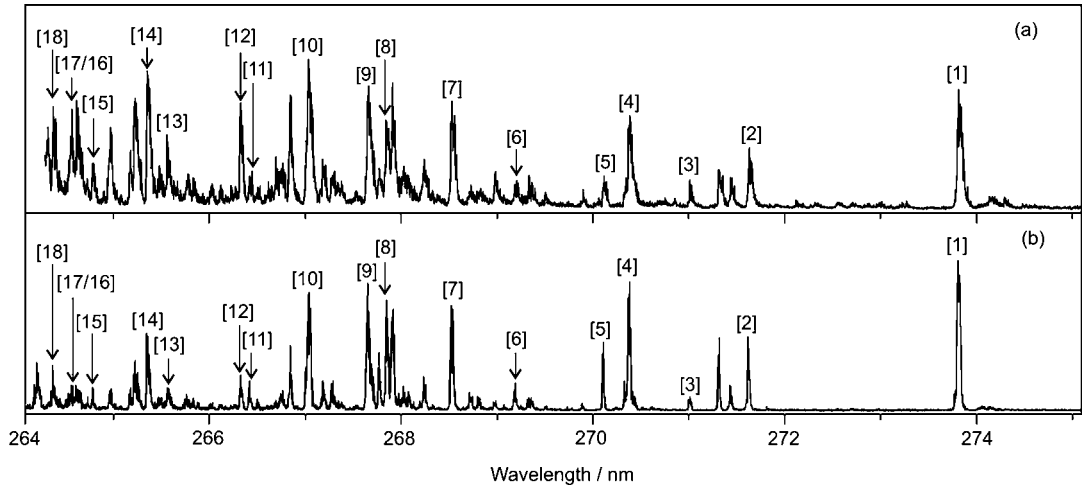

Figure 2. (a) 1 + 1 REMPI spectrum for forming parent phenol-d_5^+ ions (m/z 99) and (b) PHOFEX spectrum for forming H atom products in the wavelength range 275 ≥ λ_{phot} ≥ 264 nm. Individual resonances, assigned with reference to Bist et al.[19] and the H (Rydberg) atom PTS studies described below, are listed in Table 1.

TABLE 1: Assignments of Peaks Highlighted in Fig. 2, Detailing the Identity and Vibrational Energies (E_{vib}) of the $^1\pi\pi^*$ Levels of Phenol-d_5 that Enhance the 1 + 1 REMPI Probability in the Displayed Wavelength Range. Assignments come Principally from Bist et al.[19] but also from the Recorded Phenol-d_5 TKER Spectra

label in Figure 2	λ_{phot}/nm	$\tilde{\nu}_{phot}$/cm^{-1}	$S_1 \leftarrow S_0$ transition	E_{vib}/cm^{-1}
[1]	273.815	36521	Origin	0
[2]	271.62	36816	$16a_0^2$	295
[3]	271.013	36898	$18b_0^1$	377
[4]	270.379	36985	$6a_0^1$	464
[5]	270.106	37022	$6b_0^1$	501
[6]	269.181	37149	τ_{OH}^1	628
[7]	268.531	37239	12_0^1	718
[8]	267.854	37333	$18a_0^1$	812
[9]	267.652	37361	$9a_0^1$	840
[10]	267.044	37447	$1_0^1/6a_0^2$	926
[11]	266.411	37536	$16a_0^2 12_0^1$	1015
[12]	266.330	37547	τ_{OH0}^1	1026
[13]	265.568	37655	$16a_0^2 9a_0^1$	1134
[14]	265.353	37685	$7a_0^1$	1164
[15]	265.221	37704	$6a_0^1 12_0^1$	1183
[16]	264.964	37741	$6b_0^1 12_0^1$	1220
[17]	264.783	37767	$9b_0^1 6b_0^1$	1246
[18]	264.369	37826	$6a_0^1 9a_0^1$	1305

spectra were also recorded at several shorter wavelengths in the range 238 ≥ λ_{phot} ≥ 206 nm, where the wavelength resolved REMPI and H atom PHOFEX spectra appeared devoid of structure, and at the ArF laser wavelength (193.3 nm). Spectra recorded at the long wavelengths showed no discernible sensitivity to the alignment of $\boldsymbol{\varepsilon}_{phot}$ relative to the TOF axis, whereas the early time part of the TOF spectrum recorded at λ_{phot} ~230 nm was clearly more intense when θ = 90° than when θ = 0°. As in the case of phenol-h_6,[2] the finding that these fast H atoms exhibit a negative (but nonlimiting) recoil anisotropy parameter indicates that this dissociation occurs on a time scale that is faster than the typical parent rotational period.

The measured H atom TOF spectra were converted into TKER space using eq 1

$$\mathrm{TKER} = \frac{1}{2} m_H \left(1 + \frac{m_H}{m_R}\right)\left(\frac{d}{t}\right)^2 \qquad (1)$$

where m_H (=1.0079 u) is the mass of the H atom, m_R is the mass of the cofragment (taken to be a phenoxyl-d_5 radical, i.e., m_R = 98.13 u), d is the path length from the interaction region to the detector, and t is the H atom TOF measured over this distance. d is determined by recording the TOF spectrum of H atoms resulting from the near UV photolysis of H_2S and least-squares fitting to the well characterized peaks associated with the various H + SH (X, v, N) product channels using literature values for D_0(H−SH)[30] and the diatomic term values.[31]

The H atom TOF (and the TKER) spectra obtained from photolysis of phenol-d_5 at any given λ_{phot} are qualitatively similar to those reported previously for phenol-h_6[2] but differ in a number of revealing details. Figure 3 compares TKER spectra derived from H atom TOF data measured following excitation of phenol-h_6 and phenol-d_5 at, respectively, their $S_1 \leftarrow S_0$ origins (Figure 3a,b), at λ_{phot} = 230 nm (Figure 3c,d) and at λ_{phot} = 193.3 nm (Figure 3e,f). In both cases, O−H bond fission following excitation to the $^1\pi\pi^*$ state occurs via coupling to the first $^1\pi\sigma^*$ PES, resulting in a structured feature centered at TKER ~6000 cm^{-1} or ~11 500 cm^{-1}, depending on whether photon absorption promotes the molecules to energies below or above the first $^1\pi\pi^*/^1\pi\sigma^*$ CI. All spectra exhibit an additional broad unstructured feature, peaking at TKER ~2000 cm^{-1}. The pedestal extending several hundred cm^{-1} beyond the fastest sharp feature in the spectra obtained at long λ_{phot} (Figure 3a,b) is most plausibly attributed to dissociation following excitation of parent hot bands that overlap the origin transition. Figure 3 illustrates several noteworthy features. The relative intensities of the fast, structured channel and the slow, unstructured signal observed from phenol-d_5 and phenol-h_6 at any given photolysis wavelength are similar, implying that most of the low TKER signal observed in the present work must be associated with O−H bond fission. Attempts to record D atom TOF spectra from phenol-d_5 photolysis at several different λ_{phot} were hampered by very low signal levels, confirming the low propensity for C−D bond fission. Second, as noted in the earlier studies of phenol-h_6 photolysis,[2] the maximum of the slow feature shifts to lower TKER as λ_{phot} is reduced from that of the S_1−S_0 origin (273.815 nm in the case of phenol-d_5) to 230 nm. Third, the TKER spectra obtained from H atom TOF measurements following photolysis of both phenol-h_6 and phenol-d_5 at λ_{phot} = 193.3 nm show an additional (structured) feature at TKER ~5000 cm^{-1}, as illustrated in Figure 3e,f. This hitherto unobserved feature is attributable to formation of phenoxyl-d_5

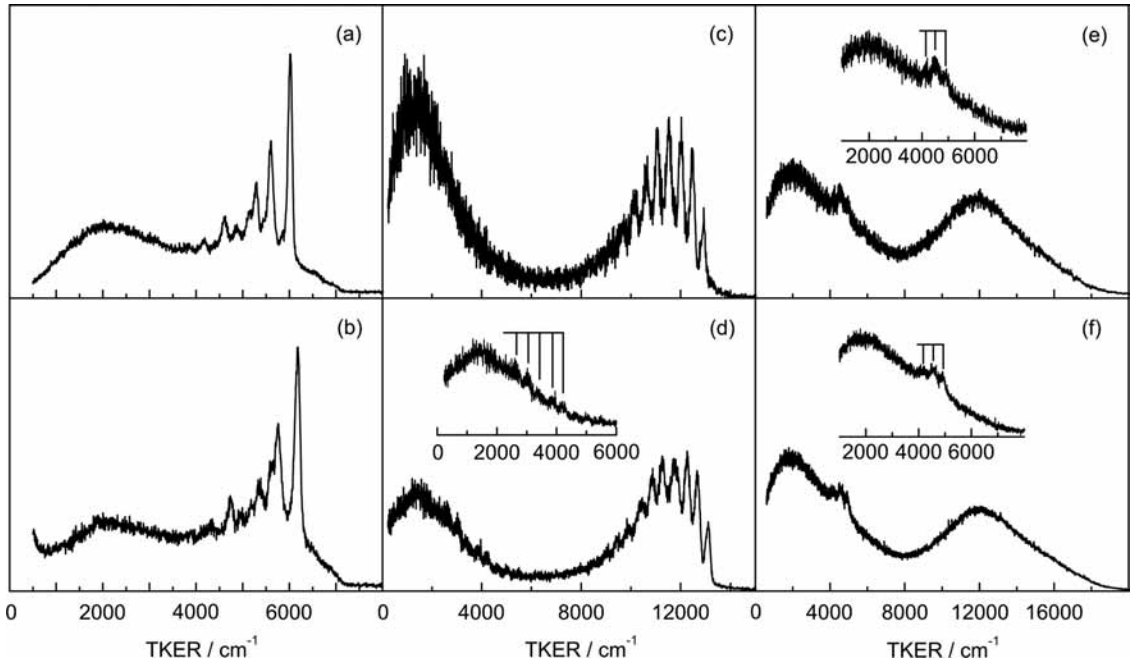

Figure 3. TKER spectra from (a) phenol-h_6 following photolysis at $\lambda_{phot} = 275.113$ nm, (b) phenol-d_5 at $\lambda_{phot} = 273.815$ nm (i.e,. at the respective S_1-S_0 origins), (c) phenol-h_6 and (d) phenol-d_5 at $\lambda_{phot} = 230$ nm, and (e) phenol-h_6 and (d) phenol-d_5 at $\lambda_{phot} = 193.3$ nm. $\boldsymbol{\varepsilon}_{phot}$ was aligned at $\theta = 90°$ in (a)−(d), while in (e) and (f), $\boldsymbol{\varepsilon}_{phot}$ was aligned at $\theta = 0°$. The insets in panels (d)−(f) show the weak structures evident in these spectra at lower TKER (∼4000−5000 cm^{-1}) on an expanded scale.

(-h_5) products in their second ($\tilde{B}^2A_2$) excited state,[29] following dissociation on the second $^1\pi\sigma^*$ PES.

We now seek to assign the vibronic structure evident in the spectra resulting from phenol-d_5 photolysis, and to compare it with that seen in the previous PTS studies of phenol-h_6.[2] Such analyses require knowledge of the (anharmonic) normal mode wavenumbers of the phenoxyl-d_5 radical. These have been calculated using Gaussian 03[32] at the DFT/B3LYP/6-311+G** level of theory and are listed in Table 2 (labeled using the Wilson notation[12]). Anharmonic wavenumbers for the 33 normal modes of the ground state phenol-d_5 parent are included in Table 2 also, along with the available experimental values,[19,33] to illustrate the predictive reliability of such calculations. Gaussian 03 calculations at this level of theory appear to replicate the experimental values best in the case of the phenol-d_5 molecule. [This same level of theory was used in our previous study of phenol-h_6 also, for the same reason, though not reported as such in the earlier publication.[2]] Before considering the spectral assignments in detail, we note that assigning the fastest peak in TKER spectra recorded at long and short λ_{phot} (e.g., Figure 3b,d) to formation of H atoms plus phenoxyl-d_5 fragments in their v = 0 level leads to contradictory values of the O−H bond strength, $D_0(H-OC_6D_5)$. As in phenol-h_6,[2] however, internal consistency can be achieved by assigning the fastest peak observed in the spectra formed at long and short λ_{phot} to formation of phenoxyl-d_5 fragments with, respectively, $v_{16a} = 1$, and $v_{16b} = 1$. Given such assignments, we obtain $D_0(H-OC_6D_5) = 30030 \pm 40$ cm^{-1} from eq 2

$$D_0(H-OC_6D_5) = E_{phot} - TKER - E_{int} \qquad (2)$$

where E_{phot} is the photon energy and E_{int} is the internal energy of the phenoxyl-d_5 fragments. This value is entirely compatible with that determined previously for the O−H bond strength in phenol-h_6, $D_0(H-OC_6H_5) = 30015 \pm 40$ cm^{-1}.[2] For ease of comparison, subsequent spectra are presented and discussed in E_{int} space, derived using the above value of $D_0(H-OC_6D_5)$.

Figure 4 shows six E_{int} spectra obtained when phenol-d_5 is excited at long λ_{phot}, corresponding to different vibronic features within the $S_1 \leftarrow S_0$ transition. Activity in fragment modes ν_{16a} and ν_{18b} (the C−O in-plane "wag") is observed at all excitation wavelengths, such that all identified product states have a″ vibrational symmetry, as in the corresponding photolyses of phenol-h_6.[2] However, there are also noteworthy differences in the product energy disposal from photolysis of phenol-d_5 and phenol-h_6, even with excitation at the respective S_1-S_0 origins. For example, the E_{int} spectrum from phenol-h_6 excitation at its S_1-S_0 origin shows a short (odd quanta only) progression in ν_{16a}, whereas that from phenol-d_5 shows no obvious feature attributable to $v_{16a} = 3$. Rather, as Figure 4a shows, the additional features in the E_{int} spectrum from phenol-d_5 photolysis at the S_1-S_0 origin are most readily assigned to population of the in-plane ring twist mode ν_{6b} and the ring breathe/C−O stretch mode ν_{19a}, both in combination with $v_{16a} = 1$. In hindsight, it is possible that part (or all) of the intensity of the feature previously assigned as $v_{16a} = 5$ in the E_{int} spectrum from phenol-h_6 photolysis could be attributable to population of the $v_{16a} = 1 + v_{19a} = 1$ mode of phenoxyl-h_5, due to the near degeneracy of $v_{16a} = 4$ and $v_{19a} = 1$. However, the relative population of product mode $v_{16a} = 3$ is unarguably much greater in the case of phenol-h_6 photolysis.

As in the earlier phenol-h_6 studies,[2] a range of behaviors is observed following excitation at energies close above the S_1-S_0 origin. For example, vibrational excitation in the photoexcited S_1 molecules can act as a "spectator" to the fragmentation process, and map through as population of the corresponding mode in the resulting radical products. In other cases, however, the parent vibration evolves into a different mode in the eventual radical or is lost completely (and thus contributes to the product TKER). Viewing spectra as in Figure 4 allows a clear comparison of the vibrational energy disposal, since population

TABLE 2: Calculated Anharmonic Wavenumbers for the Normal Mode Vibrations of Phenol-d_5 and the Phenoxyl-d_5 Radical, Calculated Using Density Functional Theory at the DFT/B3LYP/6-311+G Level (With Anharmonic Corrections), and the Gaussian 03 Computational Suite[32,a]**

	phenol-d_5			phenoxyl-d_5	
mode	symmetry	anharmonic wavenumber/cm^{-1}	expt/cm^{-1} (refs 33 and 19)	symmetry	anharmonic wavenumber/cm^{-1}
O−H stretch	a′	3637	3656/2700	disappearing mode	
20a	a′	2284	2281/2313	a_1	2283
2	a′	2240	2258/2295	a_1	2278
13	a′	2262	2249/2262	a_1	2268
8a	a′	1580	1567/1572	a_1	1506
19a	a′	1391	1404/1405	a_1	1416
7a	a′	1190	1204/1187	a_1	1240
O−H bend	a′	1168	1179/1179	disappearing mode	
1	a′	956	960/960	a_1	936
18a	a′	882	837/840	a_1	856
9a	a′	839	869/879	a_1	830
12	a′	754	756/754	a_1	719
6a	a′	517	513/513	a_1	511
20b	a′	2273	2262/2302	b_2	2288
7b	a′	2253	2294/2283	b_2	2260
8b	a′	1576	1579/1578	b_2	1441
19b	a′	1309	1372/1372	b_2	1331
3	a′	1365	1021/1021	b_2	1237
14	a′	1018	1301/1300	b_2	1031
9b	a′	844	813/831	b_2	847
15	a′	816	-/810	b_2	809
6b	a′	590	594/595	b_2	568
18b	a′	387	386/386	b_2	421
17a	a″	844	776/766	a_2	853
10a	a″	639	636/694	a_2	616
16a	a″	361	357/358	a_2	327
5	a″	785	831/825	b_1	787
17b	a″	775	754/720	b_1	781
10b	a″	629	624/625	b_1	663
4	a″	555	550/550	b_1	496
16b	a″	436	430/431	b_1	415
O−H torsion	a″	290	307/307	disappearing mode	
11	a″	213	232/231	b_1	172

[a] The calculated anharmonic wavenumbers for phenol-d_5 are compared with the fundamentals derived from experiment (from refs 19 and 33). Modes are quoted using the Wilson mode labelling scheme[12] and ordered on the basis of the C_{2v} symmetry labels of the phenoxyl-d_5 products.

of any particular mode of the phenoxyl-d_5 product will be revealed at the appropriate E_{int}, irrespective of E_{phot}. None of the photolyses yield phenoxyl-d_5 products in their $v = 0$ level (i.e., fragments with $E_{int} = 0$). Excitation on the S_1-S_0 $16a_0^2$ transition results in population in product modes ν_{16a}, ν_{11}, and (possibly) ν_{18b} as shown in Figure 4b. The corresponding excitation in phenol-h_6 resulted in formation of phenoxyl-h_5 products carrying vibrational excitation in the first two of these modes, and in ν_{6a}. As with excitation at the S_1-S_0 origin, the observed progression in odd quanta of product mode ν_{16a} is less extensive in the case of phenol-d_5 photolysis than for phenol-h_6.

Parts c, d, and e of Figure 4 display E_{int} distributions in the phenoxyl-d_5 fragments resulting from excitation on the S_1-S_0 $6a_0^1$, $6b_0^1$ and 12_0^1 resonances of phenol-d_5. Each reveals a strong propensity for retention of the excited parent mode in the eventual radical products; the dominant peak in the respective E_{int} profiles is assignable to one quantum of the photoprepared "spectator" mode in combination with $v_{16a} = 1$. Weaker peaks attributable to $v_{16a} = 1$ reveal some probability for the vibration to be lost to kinetic energy. Similar behavior was observed following excitation via the S_1-S_0 $18b_0^1$, $9a_0^1$ and $1_0^1(6a_0^2)$ transitions. In all such cases, the TKER/E_{int} peak assignments serve to reinforce the 1 + 1 REMPI spectral assignments given in Table 1 (and vice versa). In other cases, however, the excited parent mode appears to couple efficiently into product translation; excitations demonstrating such behavior include the S_1-S_0 $18a_0^1$ (Figure 4f) and $7a_0^1$ transitions. Note how these assignments, involving a limited set of fundamentals, serve to validate the product mode assignments given following excitation at the phenol-d_5 S_1-S_0 origin. The dominant peak in the E_{int} spectrum obtained with excitation at the S_1-S_0 $6b_0^1$ transition (Figure 4d), for example, is attributable to phenoxyl-d_5 products with $v_{6b} = 1$ (together with $v_{16a} = 1$). It falls at the same E_{int} as a feature in the spectrum obtained with excitation at the S_1-S_0 origin, which is assigned accordingly (Figure 4a).

Figure 5 shows E_{int} spectra obtained following dissociation of phenol-d_5 at λ_{phot} = (a) 234 nm, (b) 230 nm, (c) 224 nm, and (d) 222 nm, i.e., at excitation energies above the first $^1\pi\pi^*/^1\pi\sigma^*$ CI. These E_{int} spectra are very similar to those recorded for phenol-h_6 and phenol-d_6 at these same short wavelengths.[2] As noted previously, internally consistent O−H bond strengths for both phenol-h_6 and phenol-d_5 are only obtained if the feature at highest TKER (lowest E_{int}) is assigned to $v_{16b} = 1$, suggesting a role for parent mode ν_{16b} in promoting coupling at the $^1\pi\pi^*/^1\pi\sigma^*$ CI. Each spectrum shows a series of peaks which are most plausibly assigned to progressions in ν_{18b} built on a progression of ν_{19a}. The corresponding E_{int} spectra resulting from photolysis of phenol-h_6 were originally assigned to a single long progression in ν_{18b}[2] but, given the near-degeneracy of ν_{19a} and $3\nu_{18b}$ in

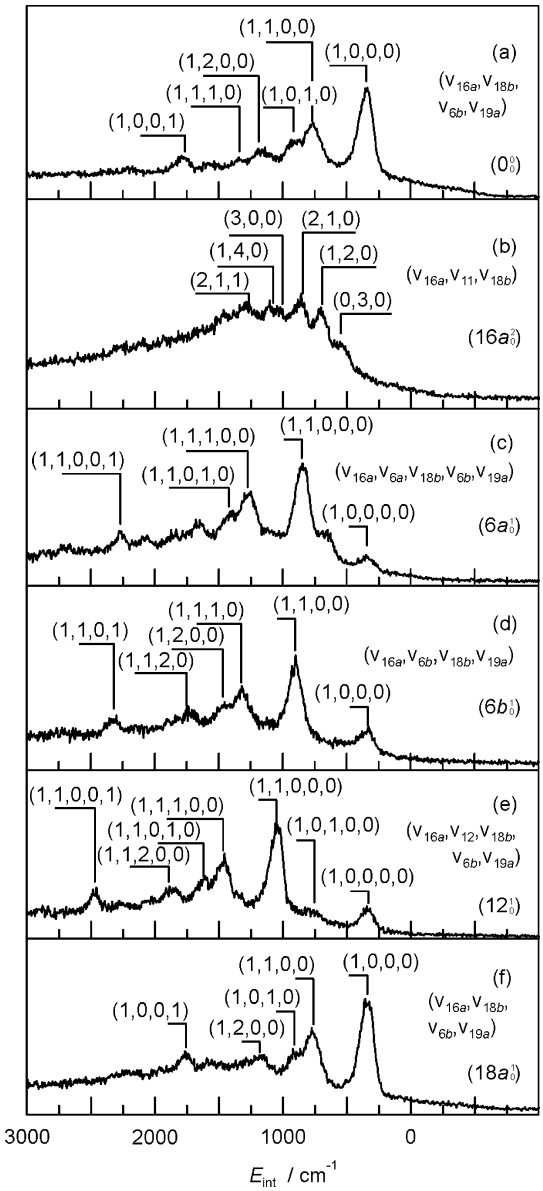

Figure 4. E_{int} spectra of the phenoxyl-d_5 products resulting from photolysis of phenol-d_5 at λ_{phot} = (a) 273.815 nm, (b) 271.620 nm, (c) 270.379 nm, (d) 270.106 nm, (e) 268.531 nm, and (f) 267.854 nm, resonant with the S_1-S_0 0_0^0, $16a_0^2$, $6a_0^1$, $6b_0^1$, 12_0^1, and $18a_0^1$ transitions, respectively. Peak assignments follow from the calculated anharmonic vibrational wavenumbers of the phenoxyl-d_5 radical listed in Table 2. In all cases, $\boldsymbol{\varepsilon}_{phot}$ was aligned at $\theta = 90°$.

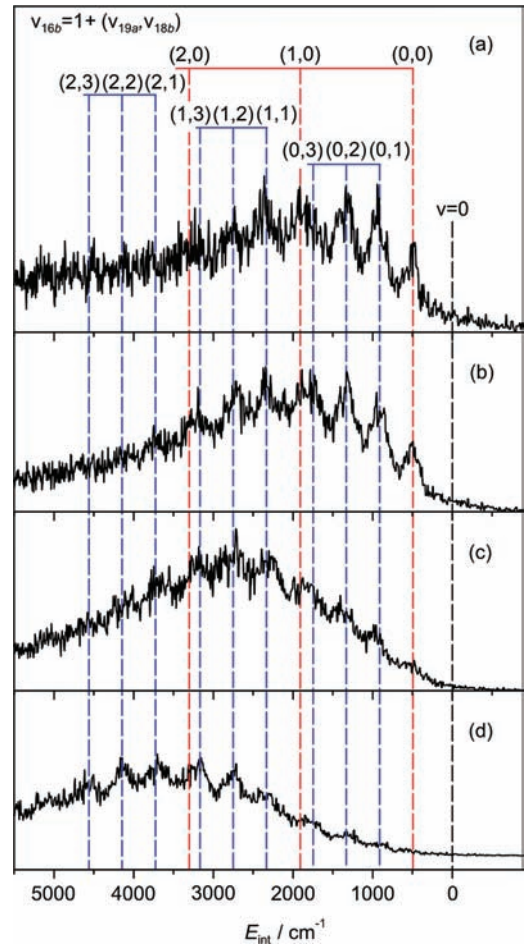

Figure 5. E_{int} spectra of the phenoxyl-d_5 fragments resulting from photolysis of phenol-d_5 at λ_{phot} = (a) 234.0 nm, (b) 230.0 nm, (c) 224.0 nm, and (d) 222.0 nm. The dashed combs indicate the product state internal energies predicted using the calculated anharmonic wavenumbers for phenoxyl-d_5 radicals listed in Table 2. In all cases, $\boldsymbol{\varepsilon}_{phot}$ was aligned at $\theta = 90°$.

the phenoxyl-h_5 radical (which is reduced in phenoxyl-d_5), the alternative assignment offered here is more likely to apply in the case of phenol-h_6 also. Some of the TKER spectra recorded in this wavelength range show hints of structure within the low TKER feature also, as illustrated for the λ_{phot} = 230 nm case (Figure 3d, inset). The high TKER limit of this structure correlates well with that expected for formation of phenoxyl-d_5 products in their first excited ($\tilde{A}^2B_2$) electronic state (given $T_{00}(\tilde{A}^2B_2-\tilde{X}^2B_1) \sim 8000$ cm^{-1} (ref 29)). It is thus tempting to regard this weak structure as indicating some branching into the H + phenoxyl-d_5 ($\tilde{A}^2B_2$) product channel, as a result of coupling via the first $^1\pi\pi^*/^1\pi\sigma^*$ CI, evolution on the $^1\pi\sigma^*$ PES and further nonadiabatic coupling at the $^1\pi\sigma^*/^1\pi\pi$ CI at large R_{O-H}.

TKER spectra recorded following photolysis of phenol-d_5 and phenol-h_6 at λ_{phot} = 193.3 nm (Figure 3e,f) display an envelope at high TKER, attributable to O−H bond fission yielding ground state phenoxyl-d_5 (-h_5) fragments, following coupling at the first $^1\pi\pi^*/^1\pi\sigma^*$ CI. These spectra also show an additional, weak feature at TKER ~5000 cm^{-1}. This feature, which is most notable when $\boldsymbol{\varepsilon}_{phot}$ is aligned at $\theta = 0°$, shows reproducible fine structure, as shown on an expanded scale in the insets to Figure 3e,f. Again, the observation of such structure is consistent with selective population of just a few product vibrational states, and thus with parent dissociation on a repulsive excited state PES. Given $D_0(H-OC_6D_5)$, the measured TKER implies $E_{int} \sim$ 16 800 cm^{-1}. This value matches well with the documented term value for the second ($\tilde{B}^2A_2$) excited electronic state of the phenoxyl radical: $T_{00}(\tilde{B}^2A_2-\tilde{X}^2B_1) \sim 16\,360$ cm^{-1} (ref 29). The observed structure is thus attributed to formation of this excited radical, in low vibrational states, following coupling to, and dissociation on, a higher $^1\pi\sigma^*$ PES as illustrated in Figure 1. The structure is less well resolved than that observed in the channel leading to ground state phenoxyl-d_5 (-h_5) fragments at longer λ_{phot}, but the peak spacing (~350 cm^{-1}) again hints at a progression in product mode ν_{18b}.

5. Discussion

The present studies of phenol-d_5 photolysis serve to confirm, and extend, insights and conclusions derived from previous studies of phenol-h_6,[2] 4-fluorophenol[14] and 4-, 3-, and 2-meth-

ylphenol.[15] Analysis of the product state distributions resulting from phenol-d_5 photolysis at many different UV wavelengths yields an internally consistent value for the O−H bond strength, $D_0(H-OC_6D_5) = 30\,030 \pm 40$ cm^{-1}, if the peaks at highest TKER in spectra recorded in the "long" and "short" wavelength regions are assigned to population of, respectively, product modes $v_{16a} = 1$ and $v_{16b} = 1$. Both of these modes involve out-of-plane ring distortions (in the fragment and the corresponding parent molecule) and, as such, have the appropriate a″ symmetry to facilitate coupling to the repulsive $^1\pi\sigma^*$ PES at the relevant CIs. However, theory[9,10] indicates that OH torsion around the C−O bond is the dominant first-order coupling mode at these CIs, and the activity in fragment modes ν_{16a} and ν_{16b} is probably better pictured as a consequence of intermode mixing in the vicinity of the CIs, reflecting the multidimensionality of the PESs and their couplings.

O−H bond fission in phenols at long wavelengths proceeds via IC from the photoexcited $^1\pi\pi^*$ state to ground state levels involving sufficient O−H stretching excitation to couple to the $^1\pi\sigma^*$ PES via the lower cone of the $^1\pi\pi/^1\pi\sigma^*$ CI at extended R_{O-H}. Possible S_0 acceptor levels for such O−H bond fission (henceforth represented as $S_0^{\#}$) are the OH stretch overtones themselves, and combination modes built on such overtones. Given that the calculated wavenumber separation between successive OH stretch overtones in the $^1\pi\pi$ potential at the energy of the S_1 origin is >1000 cm^{-1},[34] the latter—i.e., OH stretch overtones in combination with low frequency symmetric (a′) vibrations—must be dominant among those states having sufficient energy in OH stretching motion to be capable of O−H bond fission. Factors determining which particular $S_0^{\#}$ level (or levels) will be populated following excitation on any given S_1-S_0 resonance and subsequent IC will include the extent of any energy mismatch between the S_1 and $S_0^{\#}$ levels (which can be accommodated if the $S_0^{\#}$ level has sufficient energy width on account of its short lifetime with respect to dissociation), and the overlap of their respective vibrational wave functions.

The earlier analyses of the S_1-S_0 absorption spectra of phenol-d_5, phenol-h_6, etc.[19] revealed which a′ modes are Franck−Condon active in vertical excitation, and thus provide a first order guide as to which modes might be expected to be Franck−Condon favored in the $S_1 \sim\!\!>\ S_0^{\#}$ IC step. Notably, all of the a′ vibrations identified in Figure 4, and in the earlier analyses of E_{int} spectra of phenoxyl-h_5 radicals resulting from long wavelength photolysis of phenol-h_6,[2] match with parent modes that are active in S_1-S_0 absorption. Thus we arrive at a rationale for the factors influencing the product vibrational energy disposal observed in the long wavelength photolysis of phenol-d_5 and in the earlier high resolution PTS studies of phenol-h_6. Photoexcitation prepares an S_1 level with specific vibrational excitation. If this excitation is in a "spectator" mode, remote from the O−H bond, it may be retained in the $S_1 \sim\!\!>\ S_0^{\#}$ IC step and in the subsequent nonadiabatic transfer at the $^1\pi\pi/^1\pi\sigma^*$ CI and map through into the eventual products. Vibronic symmetry must be conserved in the $S_1 \sim\!\!>\ S_0^{\#}$ IC step, but energy conservation may require excitation of (a′) modes additional to just the proximate OH stretch overtone. Again, if these a′ vibrations (in $S_0^{\#}$) are only weakly coupled with the breaking O−H bond, they can be expected to reveal themselves in the eventual product vibrational energy disposal.

Nonadiabatic transfer at the $^1\pi\pi/^1\pi\sigma^*$ CI involves an A′ → A″ change in electronic symmetry which, experiment shows, is compensated by an a′ → a″ change in overall vibrational symmetry. This has been discussed as an illustrative example of the geometric phase effect in a molecular photodissociation[35] and, in the case of phenol-d_5, accounts for the dominance of product states carrying one quantum of ν_{16a}—the skeletal mode which, along with the OH torsion, is most actively involved in coupling at the $^1\pi\pi/^1\pi\sigma^*$ CI. The phenoxyl-d_5 products observed in the present study display excitation in $v_{16a} = 1$ only, whereas the earlier phenol-h_6 photolysis studies[2] deduced formation of phenoxyl-h_5 products with $v_{16a} = 1$, 3, and 5. As noted earlier, the peak attributed to phenoxyl-h_5 products with $v_{16a} = 5$ could alternatively be assigned to population with $v_{16a} = 1 + v_{19a} = 1$, but the $v_{16a} = 3$ product assignment in the long wavelength photolysis of phenol-h_6 appears robust. It is not obvious why coupling at the $^1\pi\pi/^1\pi\sigma^*$ CI should generate substantially more excitation in product mode ν_{16a} in the case of phenol-h_6 than in phenol-d_5. This isotope effect might reflect subtle differences in the interplay between the various coupling modes (and thus in the nonadiabatic dynamics) at the $^1\pi\pi/^1\pi\sigma^*$ CI or could be indicative of differences in the $S_1 \sim\!\!>\ S_0$ IC step. For example, given the above discussion, the observation of phenoxyl-h_5 products with $v_{16a} = 3$ could imply that favored $S_0^{\#}$ acceptor levels in phenol-h_6 carry $v_{16a} = 2$. [Table 1, and the UV absorption studies[19] both indicate some Franck−Condon activity in the S_1-S_0 $16a_0^2$ transition]. Finally, the departing H atom will exert a tangential impulse on the O atom, which would be expected to manifest itself via population of product mode ν_{18b} (the C−O wag), as observed.

Excitation at shorter λ_{phot}, at energies above the first $^1\pi\pi^*/^1\pi\sigma^*$ CI, results in the formation of fast H + phenoxyl-d_5 ($\tilde{X}$) fragments, with the latter carrying vibrational excitation in ν_{18b} (the in-plane C−O wag), ν_{19a} (which involves a combination of in-plane ring-breathing and C−O stretching motions) and ν_{16b}. Activity in ν_{19a} and ν_{18b} can be understood in terms of forces acting as a result of the initial $\pi^* \leftarrow \pi$ excitation, and the impulse associated with the eventual O−H bond fission, respectively, while activity in ν_{16b} is considered to be a signature of the nonadiabatic coupling at the CI. The observed energy disposal parallels that deduced following H atom loss from 4-fluorophenol[14] and 4-methylphenol,[15] though ν_{7a} is identified as the favored in-plane ring-breathe/C−O stretch mode in the 4-fluorophenoxyl products. As discussed earlier, the phenoxyl-h_5 radicals resulting from phenol-h_6 photolysis at these short wavelengths almost certainly carry excitation in mode ν_{19a} also, though this was not recognized in the original analysis as a result of the near degeneracy of $3\nu_{18b}$ and ν_{19a}.[2] Some TKER spectra measured in the short wavelength range (e.g., at $\lambda_{phot} = 230$ nm, Figure 3d) show hints of additional structure which may be attributable to formation of H + phenoxyl-d_5 ($\tilde{A}$) products. The deduced branching into this excited product channel at the $^1\pi\sigma^*/^1\pi\pi$ CI would not be surprising (it is observed in the corresponding dissociation of thiophenol, for example[5]) and lends support to the interpretation of recent velocity map imaging studies of H atoms arsing in the vibrationally mediated UV photolysis of phenol-d_5.[22]

The fast H + phenoxyl-d_5 ($\tilde{X}$) product channel is still evident with excitation at $\lambda_{phot} = 193.3$ nm (Figure 3f), but the new feature to note in this TKER spectrum is the structure attributable to formation of phenoxyl-d_5 fragments in the $\tilde{B}^2A_2$ state. Similar product branching is seen when phenol-h_6 is excited at this wavelength, but not at $\lambda_{phot} = 206$ nm.[2] This attribution implies the existence of another CI in the R_{O-H} exit channel, which is open following vertical excitation with an energy ~6.4 eV and provides a route from the one (or more) optically bright bound states populated by photoexcitation at this energy to the second $^1\pi\sigma^*$ state (of $^1A''$ ($^1A_2$ in C_{2v}) symmetry), as illustrated in Figure 1. As noted earlier, this channel appears most clearly

when $\boldsymbol{\varepsilon}_{\text{phot}}$ is aligned at $\theta = 0°$, implying a positive recoil anisotropy parameter, which would be consistent with excitation to the second $^1\pi\pi^*$ state and subsequent prompt dissociation via the second $^1\pi\pi^*/^1\pi\sigma^*$ CI, as illustrated in Figure 1. It is unclear at this stage what role, if any, this $\tilde{B}$ state product channel might play in the production of prompt, slow H atoms observed in recent ultrafast pump−probe studies at $\lambda_{\text{phot}} \sim 200$ nm.[23]

Finally, the persistence of the broad feature centered at low TKER (~ 2000 cm^{-1}), which is evident in all spectra recorded with the phenol-d_5 parent, establishes that this is largely associated with an O−H bond fission—a conclusion that is reinforced by the paucity of D atom signal. Such a finding contrasts with that of Hause et al.,[22] who reported notable reductions in the slow H atom signal upon ring deuteration. These results are not necessarily contradictory, however, since one can envisage several contributory O−H bond fission mechanisms, namely, IC from the photobright $^1\pi\pi^*$ state and subsequent unimolecular decay on the S_0 PES, and a number of multiphoton induced fragmentation processes, e.g., two photon excitation to, and dissociation from, superexcited states.[13] Clearly, the relative contributions could depend sensitively on the experimental conditions (e.g., excitation wavelength and, particularly, laser pulse intensity and duration). Indeed, the low TKER feature at long λ_{phot} is centered at ~ 2000 cm^{-1}, while at shorter excitation wavelengths, this shifts to ~ 1500 cm^{-1}, hinting that multiphoton processes are more likely with excitation near the $S_1 \leftarrow S_0$ origin.

6. Conclusions

H atom loss from phenol-d_5 following excitation at many wavelengths in the range $275 \geq \lambda_{\text{phot}} \geq 193.3$ nm has been investigated using a combination of $1 + 1$ REMPI spectroscopy (at the longer excitation wavelengths) and H (Rydberg) atom PTS methods. O−H bond fission in phenol-d_5 is shown to occur via mechanisms similar to those observed for phenol-h_6, i.e., by coupling to the lowest energy $^1\pi\sigma^*$ PES either by indirect means, after IC to high vibrational levels of the electronic ground state and subsequent coupling via the $^1\pi\pi/^1\pi\sigma^*$ CI (at the longer excitation wavelengths) or, at shorter wavelengths, by nonadiabatic coupling via the first $^1\pi\pi^*/^1\pi\sigma^*$ CI.[2] Broadly similar behavior has been reported previously in the UV photolysis of 4-fluoro- and 4-chlorophenol,[14] and in 2-, 3-, and 4-methylphenol.[15] O−D bond fission in phenol-d_6, however, is only observed at excitation energies above the $^1\pi\pi^*/^1\pi\sigma^*$ CI.[2] The present work provides further illustration of the generality, and efficiency, of $^1\pi\sigma^*$ state mediated O−H bond fission following UV photoexcitation of phenols and, at the shortest excitation wavelength studied ($\lambda_{\text{phot}} = 193.3$ nm), provides the first clear evidence of dissociation via a higher energy $^1\pi\pi^*/^1\pi\sigma^*$ CI, yielding phenoxyl-h_5 (-d_5) fragments in their second ($\tilde{B}^2A_2$) excited state. It also offers additional insights into the origin(s) of the pronounced low kinetic energy feature observed in TKER spectra from photolysis of all phenols, clearly associating it with one or more O−H bond fission processes, e.g., unimolecular decay on the S_0 PES (following IC from the photoexcited $^1\pi\pi^*$ state) and/or decay from superexcited states populated via two (or more) photon absorption.

The energy resolution of the H (Rydberg) atom PTS method is sufficient to allow measurement and analysis of the vibrational energy disposal in the phenoxyl-d_5 products from photolysis of phenol-d_5, its dependence on λ_{phot}, and thus determination of the O−H bond strength, $D_0(\text{H}-\text{OC}_6\text{D}_5) = 30\,030 \pm 40$ cm^{-1}. The detailed energy disposal shows many similarities with, but also differences from, that deduced from companion studies of other isotopologues of phenol, and from substituted phenols. Specifically, neither $v = 0$ products nor any products with overall a′ vibrational symmetry are observed. All populated product states are deduced to carry a quantum of ν_{16a} or ν_{11} (if formed by indirect coupling via the $^1\pi\pi/^1\pi\sigma^*$ CI) or a quantum of ν_{16b} (when the $^1\pi\sigma^*$ PES is accessed via the first $^1\pi\pi^*/^1\pi\sigma^*$ CI), often in combination with one or more modes of a′ symmetry. Factors identified as influencing the detailed vibrational energy disposal, and its sensitivity to λ_{phot}, isotopologue, and ring substituents include: the propensity for retaining skeletal, "spectator" motions introduced in the initial parent photoexcitation and/or in the $S_1 \sim\sim> S_0^{\#}$ IC step; the a′ → a″ change in overall vibrational symmetry introduced by the nonadiabatic coupling at the respective CIs, and the tangential force exerted by the departing H atom on the O atom once the molecule has accessed the $^1\pi\sigma^*$ PES.

Acknowledgment. We are grateful to EPSRC for financial support via a Programme Grant, and to Professors R. N. Dixon and J. N. Harvey, and to K. N. Rosser, for their many and varied contributions to this work.

References and Notes

(1) Tseng, C. M.; Lee, Y. T.; Ni, C. K. *J. Chem. Phys.* **2004**, *121*, 2459.
(2) Nix, M. G. D.; Devine, A. L.; Cronin, B.; Dixon, R. N.; Ashfold, M. N. R. *J. Chem. Phys.* **2006**, *125*, 133318.
(3) Ashfold, M. N. R.; Cronin, B.; Devine, A. L.; Dixon, R. N.; Nix, M. G. D. *Science* **2006**, *312*, 1637.
(4) Tseng, C. M.; Lee, Y. T.; Lin, M. F.; Ni, C. K.; Liu, S. Y.; Lee, Y. P.; Xu, Z. F.; Lin, M. C. *J. Phys. Chem. A* **2007**, *111*, 9463.
(5) Ashfold, M. N. R.; Devine, A. L.; Dixon, R. N.; King, G. A.; Nix, M. G. D.; Oliver, T. A. A. *Proc. Natl. Acad. Sci.* **2008**, *105*, 12701.
(6) Iqbal, A.; Pegg, L. J.; Stavros, V. J. *J. Phys. Chem. A.* **2008**, *112*, 9531.
(7) Sobolewski, A. L.; Domcke, W. *J. Phys. Chem. A* **2001**, *105*, 9275.
(8) Sobolewski, A. L.; Domcke, W.; Dedonder-Lardeux, C.; Jouvet, C. *Phys. Chem. Chem. Phys.* **2002**, *4*, 1093.
(9) Lan, Z. G.; Domcke, W.; Vallet, V.; Sobolewski, A. L.; Mahapatra, S. *J. Chem. Phys.* **2005**, *122*, 224315.
(10) Vieuxmaire, O. P. J.; Lan, Z.; Sobolewski, A. L.; Domcke, W. *J. Chem. Phys.* **2008**, *129*, 224307.
(11) Creed, D. *Photochem. Photobiol.* **1984**, *39*, 537, 563, 577.
(12) Wilson, E. B. *Phys. Rev.* **1934**, *45*, 706.
(13) Schick, C. P.; Weber, P. M. *J. Phys. Chem. A* **2001**, *105*, 3725.
(14) Devine, A. L.; Nix, M. G. D.; Cronin, B.; Ashfold, M. N. R. *Phys. Chem. Chem. Phys.* **2007**, *9*, 3749.
(15) King, G. A.; Devine, A. L.; Nix, M. G. D.; Kelly, D. E.; Ashfold, M. N. R. *Phys. Chem. Chem. Phys.* **2008**, *10*, 6417.
(16) Sur, A.; Johnson, P. M. *J. Chem. Phys.* **1986**, *84*, 1206.
(17) Yamada, Y.; Ebata, T.; Kayano, M.; Mikami, N. *J. Chem. Phys.* **2004**, *120*, 7400.
(18) Kayano, M.; Ebata, T.; Yamada, Y.; Mikami, N. *J. Chem. Phys.* **2004**, *120*, 7410.
(19) Bist, H. D.; Brand, J. C. D.; Williams, D. R. *J. Mol. Spectrosc.* **1967**, *24*, 402, 413.
(20) Tripathi, G. N. R.; Schuler, R. H. *J. Chem. Phys.* **1984**, *81*, 113.
(21) Berthomieu, C.; Boussac, A. *Biospectroscopy* **2004**, *1*, 187.
(22) Hause, M. L.; Yoon, Y. H.; Case, A. S.; Crim, F. F. *J. Chem. Phys.* **2008**, *128*, 104307.
(23) Iqbal, A.; Cheung, M. S. Y.; Nix, M. G. D.; Stavros, V. G. *J. Phys. Chem. A*, submitted for publication.
(24) Cronin, B.; Nix, M. G. D.; Qadiri, R. H.; Ashfold, M. N. R. *Phys. Chem. Chem. Phys.* **2004**, *6*, 5031.
(25) Cronin, B.; Nix, M. G. D.; Devine, A. L.; Dixon, R. N.; Ashfold, M. N. R. *Phys. Chem. Chem. Phys.* **2005**, *8*, 599.
(26) Werner, H. J.; Knowles, P. J.; Lindh, R.; Manby, F. R.; Schütz, M.; Celani, P.; Korona, T.; Rauhut, G.; Amos, R. D. Bernhardsson, A.; Berning, A.; Cooper, D. L.; Deegan, M. J. O.; Dobbyn, A. J.; Eckert, F.; Hampel, C.; Hetzer, G. Lloyd, A. W.; McNicholas, S. J.; Meyer, W.; Mura, M. E.; Nicklass, A.; Palmieri, P.; Pitzer, R.; Schumann, U.; Stoll, H.; Stone, A. J.; Tarroni, R.; Thorsteinsson, T. MOLPRO, version 2006.1, a package of ab initio programs, Cardiff, U.K., 2006.
(27) Dunning, T. H. *J. Chem. Phys.* **1989**, *90*, 1007.
(28) Roos, B. O.; Andersson, K. *Chem. Phys. Lett.* **1995**, *245*, 215.

(29) Ward, B. *Spectrochim. Acta* **1968**, *24A*, 813.

(30) Cook, P. A.; Langford, S. R.; Dixon, R. N.; Ashfold, M. N. R. *J. Chem. Phys.* **2001**, *114*, 1672, and references therein.

(31) Huber, K. P.; Herzberg, G. *Constants of Diatomic Molecules*; Van Nostrand Reinhold: New York, London, 1979.

(32) Frisch, M. J. ; Trucks, G. W.; Schlegel, H. B.; Scuseria, G. E.; Robb, M. A.; Cheeseman, J. R.; Montgomery, J. A., Jr.; Vreven, T.; Kudin, K. N.; Burant, J. C.; Millam, J. M.; Iyengar, S. S.; Tomasi, J.; Barone, V.; Mennucci, B.; Cossi, M.; Scalmani, G.; Rega, N.; Petersson, G. A.; Nakatsuji, H.; Hada, M.; Ehara, M.; Toyota, K.; Fukuda, R.; Hasegawa, J.; Ishida, M.; Nakajima, T.; Honda, Y.; Kitao, O.; Nakai, H.; Klene, M.; Li, X,; Knox, J. E.; Hratchian, H. P.; Cross, J. B.; Adamo, C.; Jaramillo, J.; Gomperts, R.; Stratmann, R. E.; Yazyev, O.; Austin, A. J.; Cammi, R.; Pomelli, C.; Ochterski, J. W.; Ayala, P. Y.; Morokuma, K.; Voth, G. A.; Salvador, P.; Dannenberg, J. J.; Zakrzewski, V. G.; Dapprich, S.; Daniels, A. D.; Strain, M. C.; Farkas, O.; Malick, D. K.; Rabuck, A. D.; Raghavachari, K.; Foresman, J. B.; Ortiz, J. V.; Cui, Q.; Baboul, A. G.; Clifford, S.; Cioslowski, J.; Stefanov, B. B.; Liu, G.; Liashenko, A.; Piskorz, P.; Komaromi, I.; Martin, R. L.; Fox, D. J.; Keith, T.; Al-Laham, M. A.; Peng, C. Y.; Nanayakkara, A,; Challacombe, M.; Gill, P. M. W.; Johnson, B.; Chen, W.; Wong, M. W.; Gonzalez C.; Pople, J. A. *GAUSSIAN 03*, Revision B.04; Gaussian, Inc.: Pittsburgh, PA, 2003.

(33) Keresztury, G.; Billes, F.; Kubinyi, M.; Sundius, T. *J. Phys. Chem. A* **1998**, *102*, 1371.

(34) Dixon, R. N. Private communication.

(35) Nix, M. G. D.; Devine, A. L.; Dixon, R. N.; Ashfold, M. N. R. *Chem. Phys. Lett.* **2008**, *463*, 305.

JP9031404